Open Access

Recent Progress in Materials

LIDSEN Publishing Inc.

Original Research

Quantum Decoherence in Dense Media: A Few Examples

Erik B Karlsson *

Department of Physics and Astronomy, Uppsala University PO Box 516, SE-75120 Uppsala, Sweden; E-Mail: erik.karlsson@physics.uu.se

* **Correspondence:** Erik B Karlsson; E-Mail: erik.karlsson@physics.uu.se

Academic Editor: Sotirios Baskoutas

Special Issue: Quantum Confinement Effects in Nano Material

Recent Progress in Materials
2020, volume 2, issue 2
doi:10.21926/rpm.2002009

Received: December 29, 2019
Accepted: March 17, 2020
Published: April 13, 2020

Abstract

Decoherence is a relatively recent concept in the field of quantum mechanics. Although the pioneers of the field must have understood that loss of phase coherence in quantum superpositions is the reason underlying the appearance of definite outcomes in the quantum measurement problem, the latter was not treated in terms of decoherence until sixty years after the formulation of quantum mechanics as described in a report by Joos and Zeh in 1983 [1]. However, soon after, the theory was developed in further detail, and experiments to measure the actual decoherence rates in various systems commenced. Today, decoherence is the main concern for another reason, i.e., the fact that superposition states must be maintained undisturbed in the quantum communication systems and decoherence presents a strong limitation for their practical application.

Decoherence appears in open quantum systems, where the basic system under consideration interacts relatively strongly with an environment. Decoherence times may be as long as seconds for small atomic systems in extreme vacua, although below what is presently measurable (i.e., less than a fraction of a femtosecond) in most liquids and solids, where coupling to the surrounding molecules or atomic arrangements is strong. The relatively slow decoherence in well-isolated particle systems has been described in several

recent articles on quantum optics, while the rapid decoherence in liquids and solids has not received this kind of attention. It is the purpose of the present review to fill this gap.

Keywords
Quantum entanglement; quantum decoherence; qubits

1. Introduction

Prior to approaching the topic of quantum decoherence, it is necessary to begin with a few basic features of standard formalism in quantum mechanics. In an analogy with the description of vectors that represent positions of points in a three-dimensional (x, y, z) coordinate system in classical physics, the basis vectors $\{|s_n>\}$ for a system *S* in quantum mechanics (which could represent a single particle) fill up an n-dimensional Hilbert space H.

Each of these basis vectors is a mathematical function corresponding to an (eigen)state of the quantum system. An operator *X* acting on the basis vector $|s_n>$ produces an (eigen)value X_n, which is one of the possible results of an experiment conducted on the physical quantity represented by operator *X*. However, a general state is a superposition of the basis vectors,

$$\Psi_S = \Sigma_n \, c_n |s_n > \qquad (1)$$

where there are n possibilities for different results X_n. A measurement leads to one of these results, each having a probability of c_n^2, where the coefficient c_n is a complex number. Superposition states may appear naturally, as in the tunneling of N-atom between two positions *a* and *b* in the ammonia molecule (NH_3) stated ahead or could be created in atoms or ions through interaction with suitable electromagnetic pulses.

In order to represent two systems with different particles *S* and *S*' interacting with each other, where *S*' spans the Hilbert space H' with base vectors $|s'_m>$, the wave function $\psi_{S+S'}$ for the total system must be written as a superposition over the combined Hilbert space H ⊗ H', as presented ahead:

$$\Psi_{S+S'} = \Sigma_n \Sigma_m \, c_{nm} \, |s_n > |s'_m > \qquad (2)$$

This formula may be generalized to several-particle systems (*S* +*S*'+*S*''+.....).

If the total Hamiltonian $H = H + H' + H_{int}$ for the combined system *S* + *S*' contains an interaction H_{int} between *S* and *S*', it would introduce the coefficient $c_n c'_m$ with $n \neq m$ in this double sum. This implies that the wavefunction $\psi_{S+S'}$ is no longer separable into a product $\psi_S \times \psi_{S'}$. The two particles no longer have separate identities, and only the *entangled* wavefunction $\Psi_{S+S'}$ corresponds to physical reality.

The interaction H_{int} that results in the entanglement has different forms and basic underlying reasons. The entanglement may be mediated by a common entangling source, such as the two Rydberg atoms coupled to the same phonon vibration in the first example, or may arise when two or more particles are interacting simultaneously with a third one such as in the neutron scattering experiments which would be described ahead.

The creation of entanglement between two or more sub-systems is, therefore, a ubiquitous phenomenon. However, the entanglement of $\psi_{S+S'}$ is not observed easily, as the interactions with the system's immediate environment *E* are usually sufficiently strong to mix $\psi_{S+S'}$ with the

environment wavefunction ψ_E and generate a complex summed multi-particle wavefunction $\psi_{S+S'+E}$ within a short time. The coefficients $c_n c'_m$ ($m \neq n$) characterizing the *S + S'* entanglement are then multiplied by random phase factors to generate a total entangled function $\psi_{S+S'+E}$ and if the environment is fluctuating randomly, the coherence within the *S* system is lost practically immediately. As would be evident from the following text, it is therefore only under exceptional circumstances that the effects of the coherent quantum superposition within the local system *S* could be followed experimentally, allowing its *decoherence time* τ_{coh}, which is characterized by the decay $\exp(-t/\tau_{coh})$, to be measured.

2. Materials and Methods

2.1 Decoherence

Erich Joos and H. Dieter Zeh were the pioneers in quantitatively estimating the decoherence times τ_{coh} for the quantum objects of different sizes perturbed by different fluctuating fields [1]. In a research work reported in 1983, the authors considered two positions $\boldsymbol{x}$ and $\boldsymbol{x'}$ in a quantum object hit by a random flow of particles (or photons) with momenta $\mathbf{p}_i = \hbar\mathbf{k}_i$. The wavelength of the particles, $\lambda = 2\pi/k$, was assumed to be much larger than the distances $|\boldsymbol{x}-\boldsymbol{x'}|$ within the object. In inelastic scattering there is always a transfer of $\Delta\mathbf{k}_i = \Delta\mathbf{p}_i/\hbar$, the perturbation would generate a phase shift $\Delta\phi = \Delta\mathbf{k}_i \cdot |\boldsymbol{x}-\boldsymbol{x'}|$ between the recoils from positions $\boldsymbol{x}$ and $\boldsymbol{x'}$. After a number [ν] of such random hits, the phase relation between the wavefunctions representing the positions $\boldsymbol{x}$ and $\boldsymbol{x'}$ would gradually wash out. Using the classical random walk formula, Joos and Zeh arrived at the formula for decoherence time, which is as follows:

$$\tau_{coh} = \frac{1}{\nu k^2 |x-x'|^2} \qquad (3)$$

Numerical estimates based on this formula demonstrate that quantum coherence in a *macroscopic particle* survives only over exceedingly low times.

For instance, in a dust grain of size = 10^{-3} cm, coherence would be lost in 10^{-36} s in the air at NPT and would remain only for 10^{-27} s even in what is considered a good laboratory vacuum (with 10^5 particles per cm^3).

However, for a *single large molecule* of size = 100 Å, the estimate points at $\tau_{coh} = 10^{-17}$ s in laboratory vacuum, while for the smallest molecules of a few Å in size, the coherence times might be prolonged to microsecond range, extending up to seconds under extreme ultra-high vacuum conditions (with 10^3 particles per cm^3).

Later works have discussed the decoherence problem in greater detail compared to that mentioned earlier [1], for specific situations and with different reasons for decoherence. The book by Breuer and Petruccione [2] summarizes several of these approaches.

2.2 Decoherence in Well-Isolated Atoms and Molecules

The cleanest situations in which decoherence may be followed in real-time are observed in quantum optics experiments. Haroche and collaborators [3] used the Rydberg atoms in high-spin states (Rb ions in spin states of 50 and 51) interacting with photons in cavity experiments and demonstrated the gradual decay of entanglement when the number of photons in the cavity was increased. Torchette et al. [4] convincingly demonstrated the validity of eq. (3) with two $^9Be^+$ or

$^{25}Mg^{+}$ ions placed in traps, separated by $\Delta\alpha$ mm; here, the lowest vibrational states of the ions were quantum entangled by sharing a common electronic excitation, and a superposition state was created using an optical start pulse at a selected time point. Its probability for survival after time t [$P = \exp(-t/\tau_{coh})$] could be measured by observing the decay of an interference signal from the two Rydberg atoms.

In the diagram depicted in Figure 1, log P is plotted as a function of the product $|\Delta\alpha|^2 \times t$, which also allows a comparison among the results for different distances ($\Delta\alpha$) between the ions. The exponential decay and the scaling with $|\Delta\alpha|^2 = |x - x'|^2$ is in perfect agreement with eq. (3). The decoherence was caused by the interaction with the remaining rest molecules in the vacuum system, and its rate was demonstrated to increase when the vacuum deteriorated.

The value of decoherence time in Figure 1 is of the order of 10^{-5} s. In a recent experiment on a similar system conducted by Man et al., this time extended up to 10^{-2} s [5].

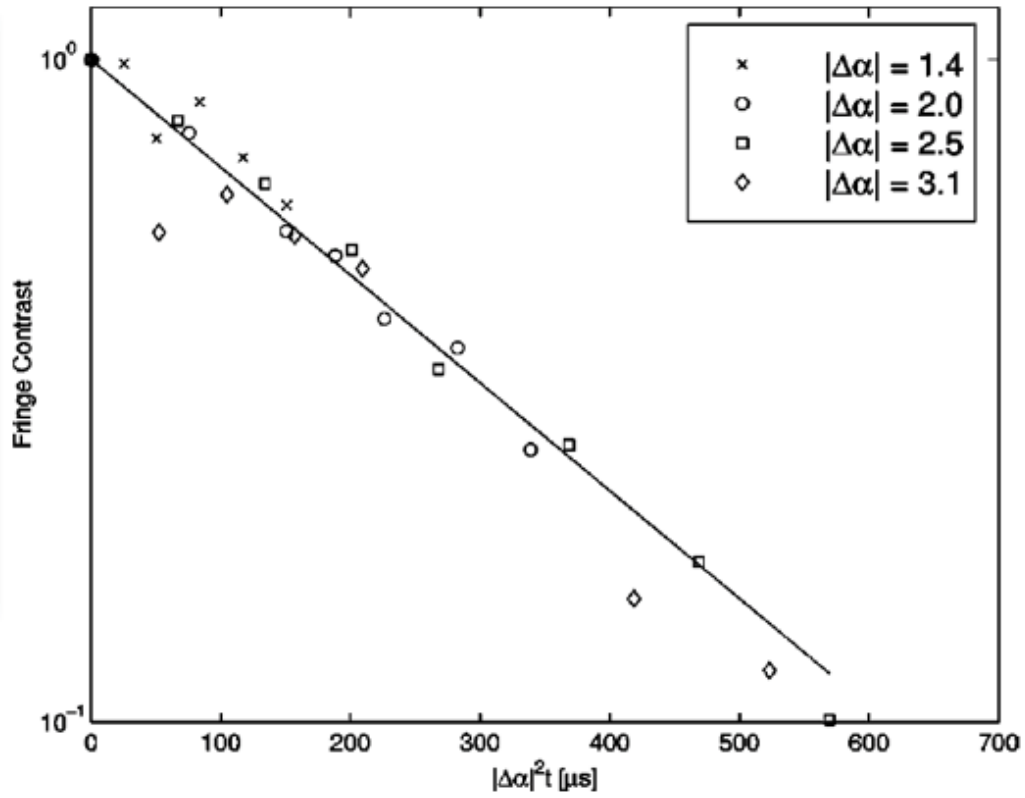

Figure 1 Decoherence in the experiment of Torchette et al. with entangled ions: Reproduced from an earlier study [4].

The states of the trapped ions in the resonance cavities are among the physical realizations of quantum bits or *qubits,* which are considered the basic elements in the attempts to construct a quantum computer. In quantum optics experiments, decoherence is weak and would not become a limiting factor, neither for the qubits themselves nor for the required entanglement among them. This is in sharp contrast to the efforts that are based on qubits in solid-state systems, as described later in the present report. However, ion trap qubits are unable to conveniently compete with solid-state qubits in terms of scalability to the multi-qubit systems.

2.3 Decoherence in Gases

2.3.1 The Ammonia Molecule

A simple example of decoherence in gases is the behavior of the ammonia molecule (NH_3) observed under different gas pressures. The N-atom may be situated on either side (*a* or *b*) of the plane defined by the three H-atoms (Figure 2).

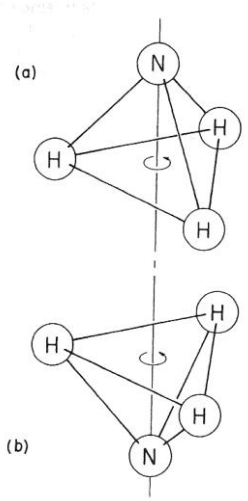

Figure 2 Two equivalent positions of the N-atom (over or below the H_3-plane) in the NH_3 molecule.

However, the corresponding quantum states $|a>$ and $b>$ overlap, and the N-atom is able to conveniently tunnel between the sites *a* and *b* as they are energetically equivalent. In regard to an isolated molecule, the ground [and the first excited state] are actually superpositions of the N atom being in positions *a* and *b*,

$$\Psi_{ge} = \frac{1}{\sqrt{2}}(|a> \pm |b>) \quad (4)$$

where g (corresponding to the + sign) represents the ground state and e (–sign) represents an excited state. The experimental evidence for this superposition is the optical activity at ν_{eg}= 24 GHz that is observed at low pressures and belongs to the transition $\Psi_g \Leftrightarrow \Psi_e$.

However, this characteristic optical signal disappears when the pressure is increased to approximately 0.5 atm, implying that at this pressure, the quantum superposition is reduced to one of the localized states $|a>$ or $b>$ through random interactions with the surrounding molecules, within a time τ_{coh} which is shorter than one optical period $2\pi/\nu_{eg}$, i.e., $\tau_{coh} \approx 10^{-10}$ s. Similar experiments conducted on the heavier deuterated molecule ND_3 have demonstrated that the tunneling state for the D-atom disappears at a pressure of 0.04 atm, while for the further heavier molecule AsH_3, no H-tunneling is observed even at the lowest attainable pressures.

In regard to this simple case, the decoherence in NH_3 may be estimated using the classical expression for the impact coefficient ν and the average momentum exerted on the molecules k at the actual temperature T and pressure p, which is as follows:

$$\nu = \sqrt{2}\pi d^2 v_{av} N_A \rho / M \quad (5)$$

With a molecular size of approximately 2 Å, $v_{av} = \sqrt{(2\,kT/M)}$, $k = Mm_p v_{av}/\hbar$ and $\rho_{NTP} = p/RT$ at $p = 0.5$ atm at room temperature, the impact coefficient z is approximately $10^8\ s^{-1}$. Eq. (4) then

predicts a decoherence time of $\tau_{coh} \approx 6 \times 10^{-11}$ s for p = 0.5 atm with an N-tunneling distance of |x–x'| = 0.85 Å, which is in the order of magnitude in agreement with the observation.

2.3.2 Hydrogen in Metals–a Lattice Gas

It is well-known that several metals absorb hydrogen and that H-atoms move so conveniently between the interstitial sites in metallic lattices that it is considered that they form a kind of "lattice gas". In a few cases, H-atoms have also been observed to tunnel between two neighboring equivalent interstitial sites in hydride crystals. In a neutron scattering experiment conducted by Magerl et al. [6], tunneling of a proton between two specific interstitial sites in Nb $(OH)_x$ was studied, and two energy separated tunneling states Ψ_g and Ψ_e were observed at low temperature, which coalesced into a single line when the temperature was raised above 5 K, where the thermal fluctuations caused strong decoherence. At these temperatures, the linewidth of neutron peaks was $\Gamma \approx 2$ meV, corresponding to a decoherence time $\tau_{coh} \approx 10^{-12}$ s, which was in agreement with the calculation, carried out by the authors, based on perturbations by the conduction electrons (since phonons are less active at these temperatures).

Tunneling of H in metallic lattices has been observed only in rare cases, although it is possible to study the process in detail when the protons are substituted with positive muons, which act as a kind of light isotope of hydrogen (with $m_\mu = 0.11\ m_p$) from a chemical perspective. The motion of positive muons in this kind of experiment is monitored by observing the muon-spin precession in the applied magnetic field. A muon spin fixed at one lattice position throughout its lifetime (which is 2.2 μsec) would be strongly dephased [7] by the static dipolar fields generated from the surrounding nuclei. In contrast, a mobile or tunneling muon would have a lower spin-relaxation as it experiences an averaged field (analogous to the motional narrowing experiments in NMR).

Figure 3 illustrates a positive muon in a metal, tunneling between two equivalent sites. The tunneling state is perturbed by phonons and the conduction electrons in the metal. Below a certain temperature (ca 5 K), the perturbation from the phonons decreases strongly (in proportion to T^{-3}), while the perturbation from the electron bath (which has a T^{-1} dependence) continues and dominates.

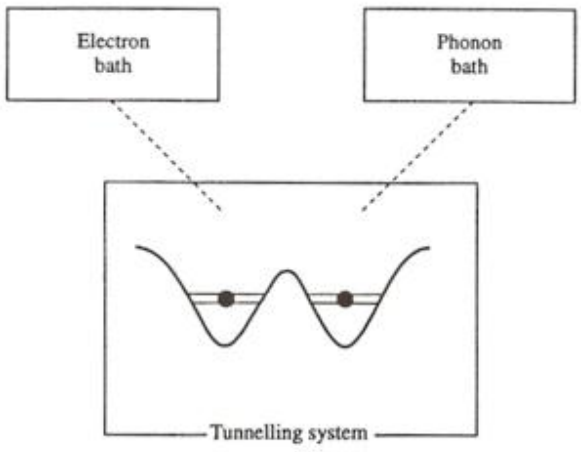

Figure 3 The tunneling system interacting with phonons and electron baths: Reproduced from [9].

The experiments conducted by Karlsson et al. [8, 9] demonstrated that it was possible to cut off the influence from the electron bath as well if the metal was converted into a superconducting one. In regard to the muons in aluminum (superconducting below T_C = 1.2 K), the tunneling was then demonstrated to be much faster below T_C (Figure 4), as the energy gap prevented the energy exchange with (and decoherence caused by) the Fermi surface electrons (Figure 5). This behavior was compared to that in the normal conducting state at the same temperature, which was achieved by quenching the superconductivity in an applied magnetic field (Figure 4).

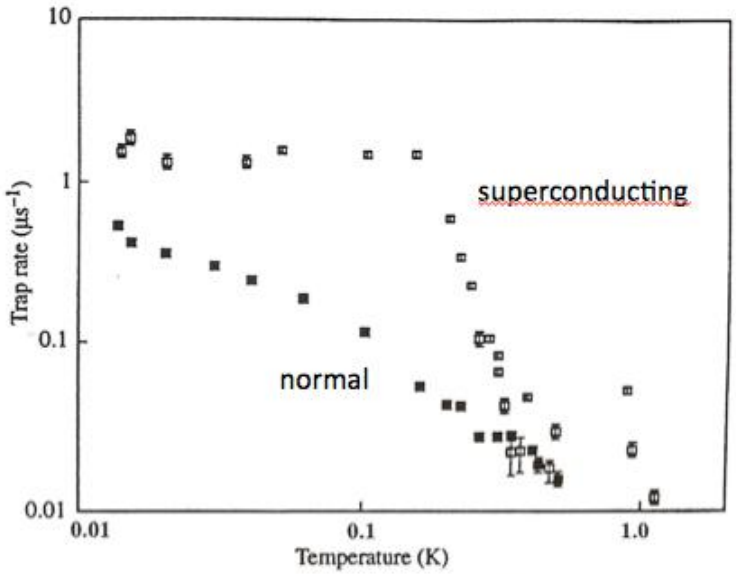

Figure 4 Muon mobility (measured as trapping rate at dilute impurities) as a function of temperature in normal and superconducting aluminum: Reproduced from ref. [9].

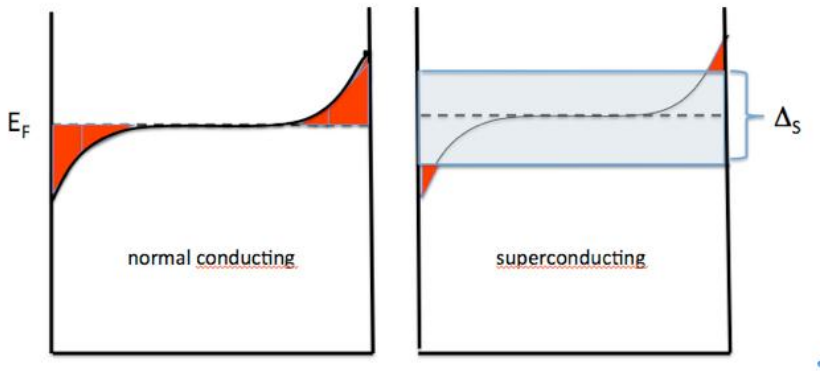

Figure 5 Tunneling probability for positive muons in Al increases strongly when the number of "active" conduction electrons (depicted in red) is decreased by opening the superconducting energy gap. Electron impulse is depicted along the horizontal axis. Reproduced from ref. [9].

Quantitatively, the decoherence time caused by conduction electrons may be written as $\tau_{coh} = \hbar/\pi KkT$, where K is the Kondo [10] factor, which has the value 0.3 for Al, leading to an estimate of $\tau_{coh} = 10^{-11}$ s for T = 1 K in the normal-conducting state. Owing to the energy gap, this time is

prolonged to $\tau_{coh} = \hbar/\pi KkTexp\ (-\Delta_s/kT)$ in the superconducting state, thereby allowing coherence between successive tunneling steps as well.

The tunneling probability decreases if there is an energy difference between adjacent potential wells, which is the case when there are impurities distorting the host metal lattice. This effect, which has certain implications on the transport in biosystems [described later in the present report], was systematically investigated in studies, using muons [11-13].

At intermediate temperatures, muons in a normal-conducting metal proceed from one tunneling position to another, although decoherence is so strong that the phase information is lost before the next tunneling step begins; this is referred to as the domain of *quantum diffusion* (Kagan and Klinger [14]). However, as stated above, a superconducting metal may allow muon *propagation* (similar to electron transport in metals), in which phase memory is maintained over several steps, and the muon is delocalized over a series of lattice sites. In order for this to occur, τ_{coh} must be much longer compared to the characteristic time-of-stay τ_{stay} in each separate double well.

Muon tunneling at temperatures above approximately 10 K is phonon-assisted, through the formation of a kind of transient muon–phonon superposition state, and has a pre-exponential $1/\sqrt{T}$ factor multiplying the classical Arrhenius law, the normal range for which is reached when over-barrier hopping sets in at higher temperature [14]. Phonon-assisted tunneling of muons was the subject of several studies in the 1980s [9]; nowadays also, it is of interest for the quantum transport of excitons in photosystems and for other biological functions (see below).

2.4 Decoherence in Liquids

2.4.1 Neutron Experiments

In the two cases stated above, naturally-occurring tunneling states served as examples of quantum superpositions and their decoherence. In other examples, such as the quantum optics experiments with the two Rydberg atoms described earlier, superpositions states were created through the interaction of two or more quantum objects with a common entangling field. The following examples of liquids and solids belong to the latter category, in which entanglement is created through interaction with an external field of radiation.

X-ray and neutron scattering are the most frequently employed methods for the detailed analysis of properties of liquids and solids at the atomic scale. The observed local spatial region depends on the longitudinal coherence length $\lambda_{\parallel}$ and the transverse coherence length $\lambda_{\perp}$ set by the spectrometer used. Together, these coherence lengths determine a coherence volume $V_{coh} = \lambda_{\parallel} \times \lambda_{\perp}^2$ selected in each scattering event. Within the (usually extremely short) coherence time τ_{coh}, the atoms within V_{coh} stay entangled with the X-ray photon or the neutron in a quantum superposition. According to eq. (3), coherence time τ_{coh} is limited by the factor $|x–x'|^2$ in the denominator, which is proportional to $(V_{coh})^{2/3}$. Decoherence strongly reduces the size of the regions, demonstrating an observable quantum entanglement.

Observation times τ_{obs} must be shorter in comparison to τ_{coh} in order to observe the evidence for entanglement and the associated decoherence. This is not a major limitation for the X-rays, for which τ_{obs} could be considered to be $c/|x–x'|$, i. e. $\tau_{obs} \approx 10^{-16}$ s for $|x–x'|$ = 10 Å. However, neutron velocities are much lower. With thermal neutrons (E $\approx$ 0.03 eV), τ_{obs} is in the time range

of 10^{-13} s, for which τ_{obs} is generally much larger than τ_{coh} and the entanglement effects are expected only in exceptional circumstances (see below). On the contrary, the faster epithermal neutrons with ≈10 eV energies, which are used in deep inelastic neutron scattering (DINS)–also referred to as neutron Compton scattering, allow observations in the time range of 10^{-15} s and below.

The next examples are derived from neutron Compton scattering on protons in liquids using DINS. A local quantum superposition of particles within the coherence volume V_{coh} is created instantly as a result of interaction with the neutron field. A coherence length of a few Å is typical under the neutron Compton scattering conditions, and at this coherence length, usually, only two or just a few particles are contained in V_{coh}. In the simple case where only two protons *a* and *b* are involved, the initial state of such an indistinguishable pair viewed by the neutron has the anti-symmetric form, represented by the following equation:

$$\Psi_i = \frac{1}{\sqrt{2}}[\phi(\mathbf{R}_{a1})\phi(\mathbf{R}_{b2}) + (-1)^{\mathrm{J}}\,\phi(\mathbf{R}_{b1})\phi(\mathbf{R}_{a2})]\chi^{\mathrm{J}}_{\mathrm{M}}(a,b)] \qquad (6)$$

where particle *a* has equal amplitudes at sites $\mathbf{R}_{a1}$ and $\mathbf{R}_{b2}$, and similar is the case for particle *b*. The spins of the two particles add up to quantum numbers J and M, which are described by the spin function $\chi^{\mathrm{J}}_{\mathrm{M}}$ (*a,b*). In the final state of Compton scattering, one of the particles recoils in the form of a plane wave, while the other one remains in its place in a molecule or in a crystal lattice. Owing to the particle indistinguishability, two interfering outgoing waves are generated, which partially cancel out each other under the influence of their zero-point vibration (see Karlsson [15]), which in turn decreases the neutron cross-section. The so-called "hydrogen cross-section anomaly" is, therefore, a result of the quantum entanglement created by the scattering neutron when interacting with two or several particles.

In the interaction with the environment, the wavefunction components of this entangled pair would, after a certain time, become mixed with those of the environmental degrees of freedom, leading to a loss of phase coherence in the superposition (6). The coupling to the environment is strong in liquids and solids, and their decoherence times are several orders of magnitude shorter than those in gases. The decoherence falls in the femtosecond range ($\tau_{coh} \approx 10^{-15}$ s), and its observation requires the use of special techniques [15].

With epithermal energies (i.e., 1–100 eV), a large fraction of the neutron kinetic energy is transferred to the scattering particles, which are consequently set free and recoil in the form of plane waves with momenta q of the order of 20–200 $Å^{-1}$ (1 $Å^{-1}$ which corresponds to a momentum of p = 1.054 × 10^{-24} kg.m/s is the unit commonly used in neutron scattering). The observation time is considered the "characteristic scattering time" τ_{sc}, which is dependent on the scattering angle θ through [16],

$$\tau_{sc} = \frac{\mathrm{M}h}{2\pi \mathrm{q}\sqrt{<\mathrm{p}>^2}} \qquad (7)$$

where M denotes the mass of the scattering nucleus, q denotes the transferred momentum (= q_1 × tan θ for protons, where q_1 is a constant), and p denotes the nuclear momentum in its thermal (or zero-point) motion when hit by the neutron.

This relationship offers a possibility for a time-differential observation. It is possible to convert the scattering probabilities N (θ) measured at different θ angles to scattering probabilities as a function of scattering time, N (τ_{sc}). In case of scattering on single, uncorrelated particles, N (θ) or N (τ_{sc}) is expected to be proportional to the particles' bound neutron cross-section σ_i, although it was first demonstrated experimentally by Dreismann et al. [17] in 1997 that this proportionality is

not valid for scattering on correlated hydrogen nuclei (i = H). The authors demonstrated the "hydrogen anomaly" stated earlier, with a strongly reduced cross-section $\sigma_{i,eff} \approx 0.6\ \sigma_i$, a reduction that was later, as stated earlier, described in ref. [15] as an effect of the strong zero-point vibrations of these light nuclei during scattering.

There exists a set of NCS observations conducted on protons and deuterons in liquids, using spectrometer settings allowing the neutron coherence volume V_{coh} to cover only two or a few protons and deuterons in the liquids. The observed quantity N (θ) is dependent on scattering angle, with small cross-section reductions $\sigma_{i,eff}/\sigma_i$ at low scattering angles, and increasingly larger reductions at higher angles. In the N (τ_{sc}) representation, this would imply that local superposition states of type (6) exist at short scattering times τ_{sc} and disappear gradually at later observation times, with a characteristic decoherence time τ_{coh} for each type of proton or deuteron environment. Figure 6 presents the data obtained for θ-dependence of neutron Compton scattering on liquid hydrogen [18]. A fit to the slope of H_2 data based on equation (7) provides a decoherence time τ_{coh} of 4 x 10^{-15} s.

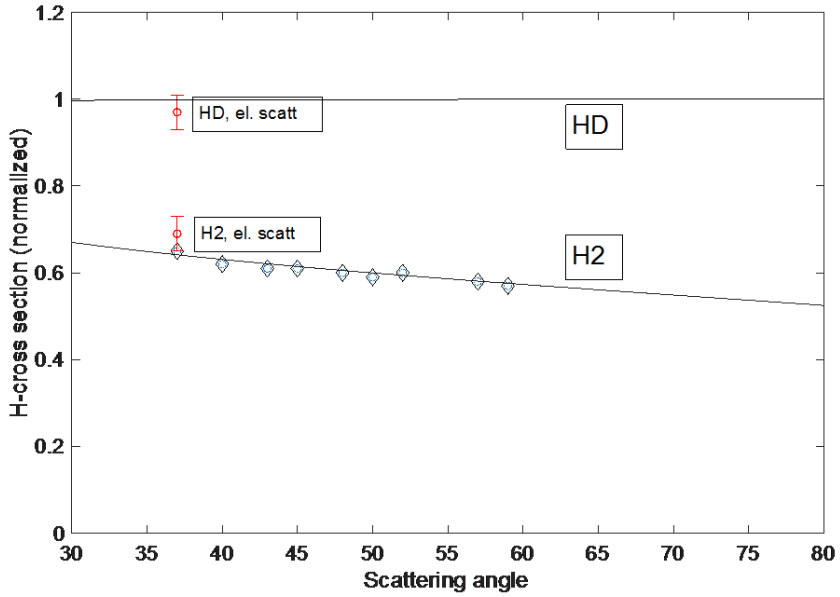

Figure 6 Data for H_2-anomalies measured with neutrons [18], fitted with theoretical predictions based on eqs. (3) and (7), providing a decoherence time τ_{coh} = 4 fs. The red points illustrate a similar electron scattering experiment conducted on gaseous H_2 and HD molecules (the latter comprising distinguishable particles, thereby showing normal cross section, as expected [19].

In case of a set of n identical particles falling within the coherence volume V_{coh} of the incoming particles [which is determined by the energy and the spatial resolution of the detecting system], each term in the multi-particle wavefunction corresponding to eq. (7) is a product of n factors among which only one contains an entangled pair (entanglement monogamy [20]), resulting in a smaller hydrogen anomaly compared to that in a pure two-particle system. The electron scattering experiment conducted by Cooper et al. [19] on gaseous H_2 (Figure 6) also demonstrated cross-section anomalies; in that study, although the coherence volume was large, it contained only one or a few molecules.

Water has also been studied using the neutron technique described above. In that study, hydrogen anomalies were also strong (again demonstrating quantum entanglement of the two water protons under the influence of the neutron), although they had a weaker angular dependence with a decoherence time of 13 ±2 fs [21]. In addition, the environment was sufficiently simple to allow a quantitative comparison with the decoherence theory, which is as follows:

The wavefunction of protons is coupled to those of the molecular vibrations, which could be of stretching $\mathbf{p}_s$ or bending $\mathbf{p}_b$ type, and in addition, there exist hydrogen bonds with the nearest surrounding H_2O molecules (Figure 7).

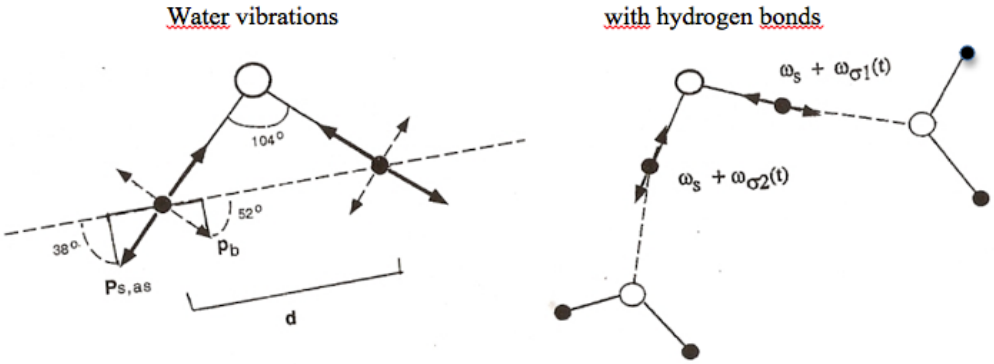

Figure 7 (a) Vibrational modes in a free water molecule and (b) Stretching vibrations modified through hydrogen bonds.

If just the lowest of these vibrations are considered, they will generate a modulation with frequency ω, but the quantum phase relations would remain in the two-proton wavefunction only as long as they are not perturbed by the fluctuating surroundings. However, when the vibrations are modified to $\omega + \omega_{\sigma 1}$ and $\omega + \omega_{\sigma 2}$, respectively, through fluctuations in the hydrogen bonds with the nearby water molecules, time-dependent terms of the type $\exp[i\{\phi + (\omega_{\sigma 2} - \omega_{\sigma 1})\}t]$ would enter in the "H_2O + Environment" wavefunction.

The factor $(\omega_{\sigma 2} - \omega_{\sigma 1})t$ changes randomly, with an R.M.S value of σ_ω, on a time scale which is of the same order of magnitude as the vibrational period itself. It is known from the vibrational spectroscopy [23] of water that the energy spread is 0.03 eV in the vibrational energy 0.46 eV, which corresponds to $\sigma_\omega \approx 0.5 \times 10^{14}\ s^{-1}$. If the distribution in σ_ω could be represented by a Gaussian function centered at $\omega_{\sigma 0}$, the mean value of the phase factor obtained would be as follows:

$$\frac{1}{\sqrt{\pi}\sigma_\omega}\int d\omega_\sigma \exp\left[-\frac{(\omega_\sigma-\omega_{\sigma 0})^2}{4\sigma_\omega^2}\right]\exp(i\omega_\sigma t) = \frac{1}{\sqrt{\pi}\sigma_\omega}\exp(-\sigma_\omega^2 t^2)\exp(i\omega_{\sigma 0}t) \quad (8)$$

where the decay factor $\exp[-\exp(-\sigma_\omega{}^2 t^2)]$ measures the decoherence. This is a Gaussian decay, although it approximates an exponential decay of $\tau_{coh} \approx 1/\sigma_\omega \approx 2 \cdot 10^{-14}$ s = 20 fs, which is in reasonable agreement outcome, 13 ± 2 fs.

2.5 Decoherence in Solids

Decoherence in solids is usually faster than the decoherence in liquids; however, exceptions do exist. Superposition states are most conveniently observed for low mass objects, the evidence for

which is the short-lived hydrogen states observed in crystals. This information is obtained exclusively from neutron scattering experiments, as protons are not easily visible in X-ray scattering. Another class of local superpositions in solids comprises the quantum states in semiconducting or superconducting materials prepared, particularly for quantum communications. A few examples from each of these areas are provided ahead.

2.5.1 Protons in Metal Hydrides as Viewed from Neutrons

Compton scattering of neutrons on the saturated yttrium hydrides YH_2 and YH_3 was studied by Karlsson et al. [24], using the technique described above for hydrogen and water. Figure 8 (left panel) presents the raw data with H-anomaly (caused by the transient entanglement of H atoms) as a function of scattering angle. These data could be fitted using decoherence time τ_{coh} = 2.0 × 10^{-15} s, although a closer analysis using the transformed dependence on time τ_{sc} (Figure 8, right-hand panel) indicated that decoherence was essentially a two-step process with a slow (or zero) initial rate in the lower range of 10^{-16} s.

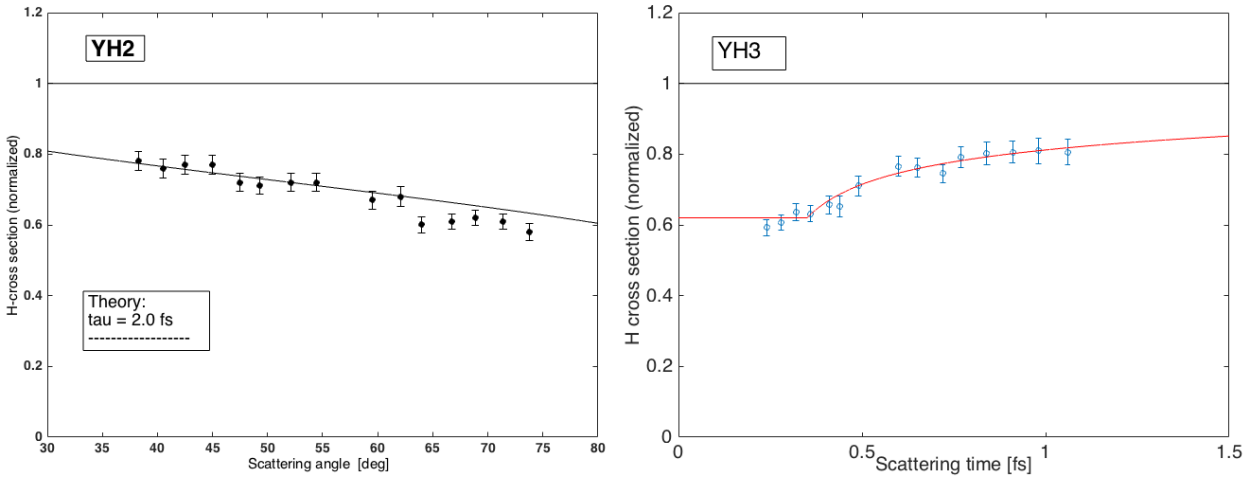

Figure 8 Hydrogen anomaly (indicating neutron-proton entanglement) in neutron scattering experiments on yttrium hydrides. Left panel: scattering-angle dependence. Right panel: scattering-time dependence, including a fixed commencement time.

The main decoherence time 2.0 fs (Figure 8) was in good agreement with the following estimate based on eq. (3): with electrons as the major source of perturbation for the protons participating in the vibrations, the typical values are k_o= 10^8 cm^{-1}, N = 10^{22}/cm^3, and v = 10^8 cm/s. Therefore, for an entangled H–H pair of size 2 Å, the Joos–Zeh formula (2) leads to a decoherence time $\tau_{coh} \approx 2 \times 10^{-15}$ s.

As stated earlier, the initial low decoherence rate was understood as a consequence of the zero-point vibrations of H atoms in the hydride. In this time range, the recoiling particle remains within the zero-vibrational range, an insight that was further corroborated by an analogous experiment conducted on deuteride YD_2. The corresponding τ_{sc}–dependence in YD_2 exhibited a further dramatic effect, with rapid initial decoherence (with $\tau_{coh} \approx 10^{-17}$ s) before the decoherence process was taken over by the 3 x 10^{-15} s rate associated with the external fluctuations stated above (Figure 9). This fast attosecond dynamics was interpreted as a consequence of the extremely strong disturbance of the lattice when the heavier deuteron

recoiled out of the YD_2 lattice, leading to extremely rapid decoherence. The 10-attosecond decay may be one of the fastest dynamic processes ever recorded in a spectroscopic measurement.

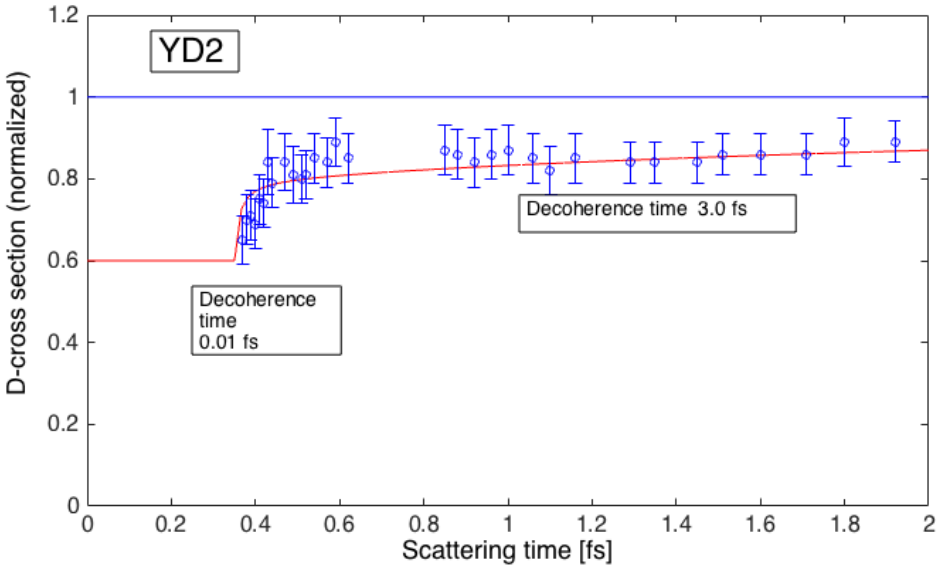

Figure 9 Cross-section anomaly for neutron scattering conducted on YD_2, in the scattering time representation.

2.5.2 Proton Dimers in Insulators as Viewed from Neutrons

As stated earlier, thermal neutron scattering is not expected to exhibit any remaining quantum superposition effects because of the associated relatively long observation times ($\approx 10^{-13}$ s). However, Fillaux and collaborators [25] demonstrated that H atoms in certain insulators containing H dimers ($KHCO_3$ and benzoic acid) could indeed remain quantum correlated over extended periods of time. Rods of scattering intensity from protons were observed at the k-values where they are not expected for non-correlated protons, and their presence could rather be explained if it was assumed that the tautomeric states were phase-correlated and remained in a quantum superposition (Figure 10).

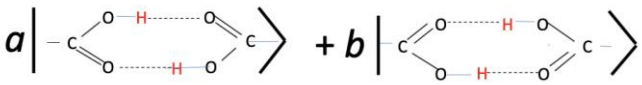

Figure 10 Superposition of the tautomeric states of protons in $KHCO_3$.

Fillaux et al. also observed that these H-peaks were stronger beyond expectation. Generally, H-scattering is almost totally inelastic because of the strong dominance of spin-flip scattering; a flip of a spin identifies the neutron path, which destroys all the interference in the scattering. However, scattering on a quantum superposition of two tautomeric dimer states (Figure 10) in $KHCO_3$ leaves the neutron paths unidentified even under the spin–flips. In addition, the Bragg peaks were narrow, indicating that the protons were not only in phase with the neighboring protons, rather all the proton pairs within the coherence volume contributed to the signal.

According to Fillaux et al., another reason for the high scattering peak intensity was the fermionic nature of the proton pairs. Because of the anti-symmetry[(compare also eq. (6) provided above) they are immune to phonon interactions for symmetry reasons and are made recoil-less. The H-sublattice is said to be super-rigid [25]. Therefore, coherence is preserved over extended periods of time. In neutron scattering, the H sub-lattice remains entangled during its interaction with the neutron over a spatial extension of a hundred or more lattice distances. Since thermal neutrons propagate with a speed of 3×10^{14} Å/s, the observation of such extended entanglements indicates that these may have decoherence times as long as $\tau_{coh} > 10^{-12}$ s. This is a kind of topological protection for coherence and entanglement.

2.5.3 Qubits in Solids

Special efforts have been dedicated to the preservation of quantum coherence in circuits constructed for future applications of quantum technology. A *qubit* is the basic element in quantum communication and computing. It is a two-state quantum superposition described by the following equation:

$$|\psi> = \alpha_0|0> + \alpha_1|1> = \frac{1}{\sqrt{2}}\left(|0> + e^{-\phi}|1>\right) \quad (9)$$

for which, the phase parameter ϕ may be determined and manipulated through interaction with an external field, similar to the Rydberg atoms in the quantum optics experiments stated earlier [3, 4]. In solids, the analogy closest to the trapped ions is the atomic or nuclear spins, which are placed in a manner that they could be addressed separately and be controlled using electromagnetic fields. Such basic elements are referred to as *spin qubits*. One requirement for successful operation is a sufficiently long coherence time for each qubit, while another is that two (or more) qubits be coupled to form entangled states which would allow processing of information in communication or computing. There are two times which are of interest here: T_1, which represents the lifetime of the excited state $|1>$ in each qubit, and T_2 (usually much shorter than T_1), which is associated with the energy spread of the levels in different qubits and causes inter-bit decoherence. When performing logical operations (swapping of spins under the action of a controlling R.F. field), entanglement is limited by T_2, which is, therefore, the effective τ_{coh} for the functioning of a computing device.

Nuclear spin states may be considerably long-lived if their environment is selected properly, as they are only weakly coupled to their surroundings. In classical NMR, the relaxation time T_1 denotes the time for the preservation of a particular nuclear spin substate, while T_2 represents the time for coherence between different nuclei in their precession in the applied magnetic field. Radiofrequency pulse sequences have been applied to create superpositions of $m_I = +½$ and $m_I = –½$ in the I = ½ spin nuclei in ^{1}H, ^{13}C, or ^{19}F isotopes used as qubits for quantum computing (Figure 11).

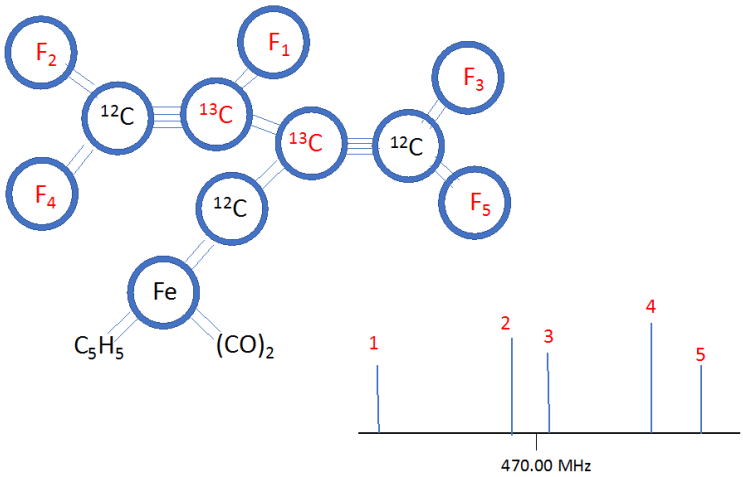

Figure 11 The molecule used for NMR-computing in ref. [26] and the signals observed from five different ^{19}F nuclei.

Single nuclear qubit coherence times may be extremely long in the liquid samples, although entanglement between them is required for logical operations that involve swapping of spin between two qubits. The inter-qubit coherence time T_2 is usually much shorter in comparison to T_1 because of the inhomogeneities or fluctuations in the local fields at different nuclei when operating with seven ±½ spin qubits (five ^{19}F nuclei and two ^{13}C nuclei), in the molecule $C_{13}O_2F_5H_5$ [27], an overall decoherence time as long as 1.3–2 s was recently reported.

However, nuclear spin qubits communicate with each other only within the same molecule (through their chemical bondings). This limits the number of qubits attainable, not allowing the construction of large-scale quantum computers. In the example described in detail in ref. [27], the number of qubits was sufficient to compute the product 3 × 5. Furthermore, large losses of signal intensity occur as all the molecules do not experience exactly the same local magnetic fields. In an attempt to overcome the latter limitation, solid-state NMR was introduced, using N-vacancies in diamond [28]. A critical evaluation of the prospects for NMR quantum computation was reported by Jones [29].

Spin qubits in the form of donor atoms doped into semiconductors can also be manipulated easily using magnetic fields and are scalable to form multi-qubit systems. However, at the same time, these are also easily perturbed by fluctuating fields in their environment. In a recent experiment conducted by He et al. [30] using phosphorous donors in silicon, the problem was not the relaxation times T_1 of the donor spins themselves [which were sufficiently long], rather the communication between the different spin qubits. The P-donors having atomic spin S = ±1/2 were placed at a distance of 150 nm using scanning tip techniques, to allow optimal conditions for swapping pairs of spins after they had been entangled by applying suitable r.f. pulses. However, the exchange interaction connecting the different donors suffered from charge noise caused by the fluctuations in their local electron screening. This was a dominant perturbation which limited the coherence time for swapping to approximately $\tau_{coh} = 10^{-8}$ s, which is a relatively short time although nonetheless sufficient for allowing a few logical operations as the swapping time itself could be reduced to 8×10^{-10} s.

Charge qubits and flux qubits operate with superconducting material, which has at least two advantages. These do not work with single charges and rather with collective bulks of coherent

superconducting Cooper pairs, which are much less sensitive to environmental perturbations compared to single charges. Their internal zero-resistance allows easier maintenance of coherence in the circuits formed. Although being macroscopic, such bulks of Cooper pairs have quantized energy states such as |0>, |1>, |2>, etc. The superconducting qubits are quantum superpositions of the two lowest among these states, |0> and |1>, prepared using suitable radiofrequency pulses.

The circuits contain one or several Josephson junctions–a few atomic layers of normal-conducting material (N) separating two superconducting (S) sections, allowing passage of Cooper pairs). These are non-linear elements that influence the separation between the energy states. The total circuit energy is a summation of charging energy $E_c\ (N_c–N_{cg})^2$, where N_{cg} is the residual charge at the gate, the Josephson junction energy is $E_J \cos\theta$, and the total Hamiltonian is provided by the following equation:

$$H = \mathrm{E_c}(\mathrm{N}_c - \mathrm{N_{cg}})^2 - \mathrm{E_J}\cos\theta \qquad (10)$$

In the realization referred to as Cooper pair box, the charging energy dominates and the corresponding memory bits are referred to as *charge qubits*. In another arrangement, referred to as the RF-SQUID, the Josephson energy dominates and the bits are referred to as *flux qubits*, as the transfer of Cooper pairs across the junction is quantized in terms of magnetic flux units $\Phi_0 = \pi h/e$.

Cooper pair boxes form a part of electronic LC circuits, in which charge and flux are quantized and their quantum states are controllable using radiofrequency pulses. Improvements have been introduced by adding parallel circuits containing additional Josephson junctions (transmon circuits), which assist in further separating the lowest qubit states |0> and |1> energetically and increasing their stability, and also by coupling the qubits to high Q-photon cavities instead of classical microwave sources (referred to as circuit QED [31]). Continued improvement in the coherence times up to $\tau_{coh} = 10^{-4}$ s was demonstrated in a recent study conducted by Kjaergaard et al. [32]. The remaining sources for decoherence are stray capacitances and local defects related to difficulties in the fabrication of small-size superconducting islands and Josephson junctions (Figure 12).

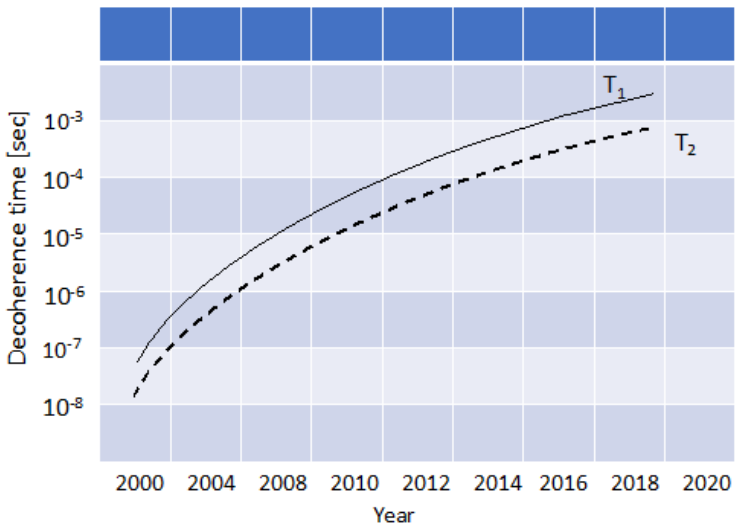

Figure 12 Improvement in coherence over time in superconducting qubits. Trends based on ref. [32].

Another two possibilities for increasing coherence times and the possibilities for error correction are as follows: (1) using feedback from an initial "weak measurement" on the system [33], and (2) storing the qubit information in a distributed way, such that it is topologically protected [34].

2.6 Macroscopic Quantum Correlations

Superconducting qubits are already a kind of macroscopic elements. However, recent quantum optics technology has allowed the demonstration of quantum behavior and entanglement between really macroscopic objects (micro-meter sized vibrating rods, weighing several grams) consisting of silicon nitride. When cooled to milli-Kelvin temperatures, the perturbations are so weak that these objects exhibit quantized vibration states and that two such vibrating objects may be coupled to form a common entangled state. The observation of these phenomena is achievable with the introduction of the field of *cavity optomechanics,* which involves photons enclosed between two mirrors. The radiation pressure generated from the photons is utilized to excite and manipulate the quantum states of the mechanical objects placed in such radiation fields. Superpositions and entanglement of macroscopic quantum states are relatively insensitive to external influence, as evidenced by the 10^{-7} s decoherence time depicted in Figure 13 (from the work of Riedinger et al. [34]).

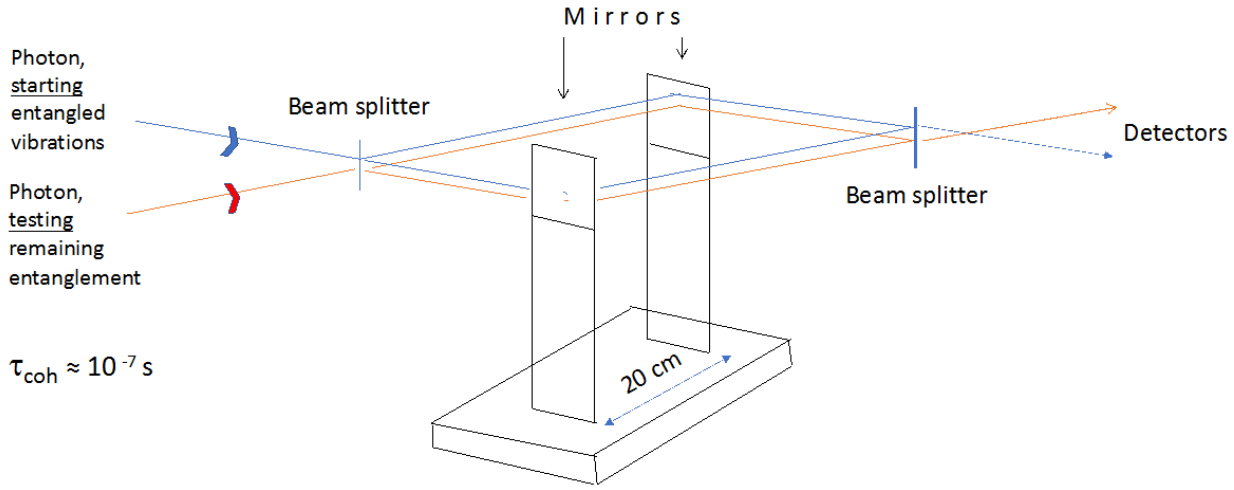

Figure 13 Two mechanical oscillators (nano-structures of SiN) placed 20 cm apart, with coinciding optical and mechanical resonances, are brought into an entangled state with the assistance of an optical pump pulse, and their degree of entanglement is read out after different delay times. Picture based on the information provided in ref. [35].

2.7 Decoherence in Biological Systems

Initially, it might appear unlikely that maintenance of quantum coherence in biological systems is possible, given the complicated structures of these systems and the strong presence of noise; however, growing evidence [36] suggests that coherence may be preserved over extended times and indeed contribute to the functioning of the processes important for living systems.

A key player in this game is the exciton, which is a bound state of an electron and an electron-hole residing on a positively charged atom, held together by electrostatic forces. Excitons are

excited by light and may have considerable extensions–both in the distance (100 Å) and time (up to 10^{-10} s)–in photosynthetic systems [36]. There are indications of even longer coherence times in cryptochromes, which are assumed to be responsible for magnetic navigation sense in birds [37, 38].

In photosystems, excitons are transferred over long distances before they reach the reaction center where they initiate a chemical process, and their motion is facilitated if they are able to proceed, by tunneling, from one local site to the next one, such as in the quantum diffusion discussed earlier for the positive muons in solids. There are indications that several such parallel paths coexist in a quantum superposition. For instance, Engel et al. observed interferences [39] in the time spectrum measured at the reaction center, which is a direct confirmation of the essential role of quantum coherences.

However, tunneling in these complicated biosystems is not expected to occur between symmetric double wells in a way it occurs for the N atom in the NH_3 molecule as described earlier or for the interstitial H-sites in pure crystals. Asymmetric tunneling requires assistance from phonons or local vibrations in the structures. What enables the coherence is actually the formation of exciton-vibrational superposition states, in which higher energy states of the excitons happen to coincide with the vibrational energies in the carrier molecules.

In their theoretical work, Caruso et al. [40] demonstrated that under such conditions, entanglement across pairs of what are referred to as Fenna-Matthew-Olson (FMO) molecular complexes, which are exciton-carriers in light-harvesting systems, could be expected to prevail for greater than 10^{-13} s.

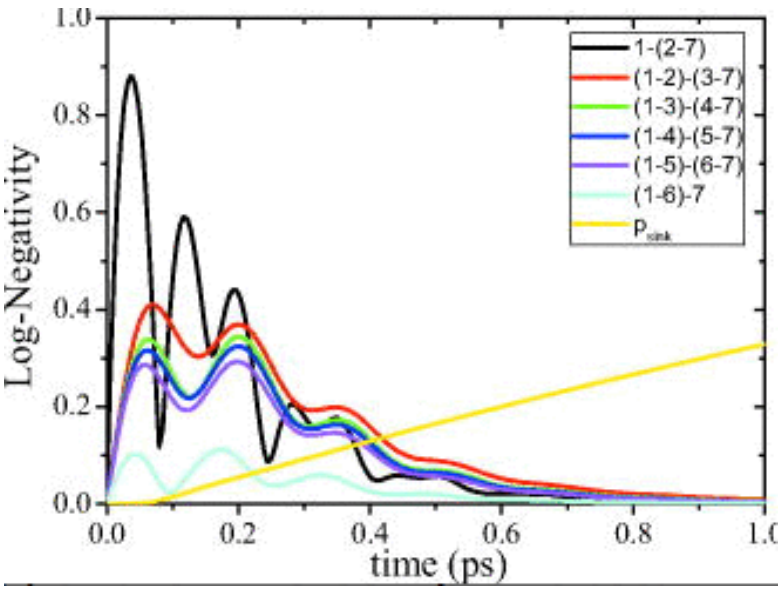

Figure 14 Calculated entanglement, measured in terms of logarithmic negativity, across the different bipartitions in the exciton-carrying FMO complex. This occurs prior to the completion of excitation transfer (yellow line). Reproduced from ref. [40].

Therefore, when the environmental fluctuations happen to be of the same order of magnitude as the energy inhomogeneities, random motion becomes a source of accidental coherence rather than producing decoherence. It appears that nature has discovered a way to accelerate the important transfer processes by exploiting the superposition principle of quantum mechanics;

living systems are based on biochemistry that allows long-distance coherent transport of charge via excitons. This mechanism appears to be the driving force behind photosynthesis, magnetic sensitivity in vision, and perhaps certain enzymatic reactions as well [36].

3. Summary

Quantum superpositions and quantum entanglement may appear over largely different time and length scales, depending on the environmental circumstances. In the present study, the measured decoherence rates ranged from several minutes for the nuclear spin-state superpositions to a few milliseconds for the ions studied under quantum optics conditions down to 10^{-17} s for deuteron pairs within a solid which are entangled in a neutron scattering process.

Figure 15 represents an attempt to display this variation for certain environmental conditions discussed above.

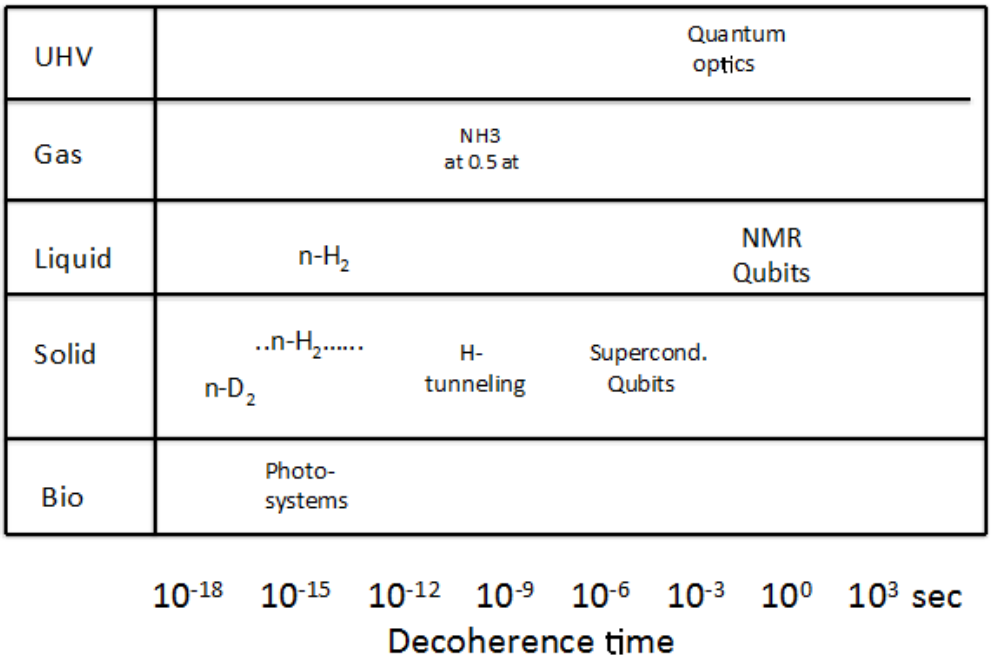

Figure 15 Overview of the variation in decoherence times in the systems discussed in the present report.

Author Contributions

Erik B Karlsson did all work.

Competing Interests

The author has declared that no competing interests exist.

References

1. Joos E, Zeh HD. The emergence of classical properties through interaction with the environment. Z Phys. 1985; B59: 223-243.

2. Breuer HP, Petruccione F. The Theory of Open Quantum Systems. Oxford: Oxford University Press; 2002.
3. Brume M, Hagley E, Dreyer J, Maitre A, Maali C, Wunderlich C, et al. Observing the progressive decoherence of the ”meter” in a quantum measurement. Phys Rev Lett. 1996; 77: 4887-4890.
4. Torchette QA, Myatt C, King J, Sackett BE, Kiepinski CA, Itano D, et al. Decoherence and decay of motional quantum states of a trapped atom coupled to engineered reservoirs. Phys Rev A. 2000; 62: 053807.
5. Man Z, Xia T, Lo Franco L. Cavity-based architecture to preserve quantum cohererence and entanglement. Nat Sci Rep. 2015; 5: 13843.
6. Magerl A, Dianoux AJ, Wipf H, Anderson IS, Neumaier K. Concentration dependence and temperature dependence of hydrogen tunneling in $Nb(OH)_x$. Phys Rev Lett. 1986; 56: 159-162.
7. Karlsson EB. Solid state phenomena, as seen by muons, protons and excited nuclei. New York: Oxford University Press; 1995.
8. Karlsson E, Wäppling R, Lidström SW, Hartmann O, Kadono R, Kiefl RF, et al. Quantum diffusion and localization of positive muons in superconducting aluminium. Phys Rev B. 1995; 52: 6217-6223.
9. Karlsson EB. The positive moun implanted in metals – a story full of surprises. Eur Phys J H. 2014; 39: 303-323.
10. Kondo J. Diffusion of light interstitials in metals. Physica B+C. 1984; 126: 279-285.
11. Cox SFJ. Implanted muon studies in condensed matter science. J Phys C. 1987; 20: 3187-3319.
12. Borghini M, Niinikoski TO, Soulié JC, Hartmann O, Karlsson E, Kehr KW, et al. Muon diffusion in niobium in the presence of traps. Phys Rev Lett. 1978; 40: 1723-1726.
13. Storchak VG, Hartmann O, Karlsson E, Wäppling R. Quantum diffusion of muons in solids. Curr Opin Sol St Mat Sci. 1999; 4: 315-320.
14. Kagan Yu, Klinger MI. Theory of quantum diffusion of atoms in crystals. J Phys. 1974; C7: 2791-2807.
15. Karlsson EB. The hydrogen anomaly problem in neutron Compton scattering. Phys Scr. 2018; 93: 035801.
16. Watson G. Neutron Compton scattering. J Phys Condens Matter. 1996; 8: 5955-5975.
17. Chatzidimitriou-Dreismann CA, Abdul-Redah T, Streffer RMF, Mayers J. Anomalous deep inelastic neutron scattering from liquid H_2O-D_2O: Evidence of nuclear quantum entanglement. Phys Rev Lett. 1997; 78: 2839-2842.
18. Chatzidimitriou-Dreismann CA, Abdul-Redah T. Attosecond entanglement of protons in molecular hydrogen: Neutron Compton scattering results. Phys B. 2004; 350: 329.
19. Cooper M J, Hitchcock AP, Chatzidimitriou-Dreismann CA. Anomalous quasielastic electron scattering from single H2, D2, and HD molecules at large momentum transfer: Indications of nuclear spin effects. Phys Rev Lett. 2008; 100: 043204.
20. Koashi M, Winter A. Monogamy of quantum entanglement and other correlations. Phys Rev A. 2004; 69: 022309.
21. Mayers J, Abdul-Redah T. Decoherence, Entanglement and information protection in complex quantum systems. NATO Science Series II. (eds. V. M. Akulin, A. Sarfati, G. Kuritzki and S. Pellegrin) Springer: 2005; 189: 555-558.

22. Karlsson EB. Effects of subfemtosecond quantum correlations in water. Phys Rev Lett. 2003; 78: 2839-2842.
23. Bratos S, Tarjus G, Diraison M, Leicknam JCI. Incoherent inelastic neutron scattering from liquid water: A theoretical study. Phys Rev A. 1991; 44: 2745-2748.
24. Karlsson EB, Hartmann O, Chatzidimitriou-Dreismann CA, Abdul-Redah T. The hydrogen anomaly in neutron Compton scattering: New experiments and a quantitative theoretical explanation. Meas Sci Technol. 2016; 27: 085501.
25. Fillaux F, Cousson A, Gutmann MJ. Macroscopic quantum entanglement and 'super-rigidity' of protons in the $KHCO_3$ crystal from 30 to 300 K. J Phys B. Condensed Matter. 2006; 18: 3229.
26. Vandersypen LMK, Steffen M, Breyta G, Yannoni CS, Sherwood MH, Chuang IL. Experimental realization of Shor's quantum factoring algorithm using nuclear magnetic resonance. Nature. 2001; 414: 883-887.
27. Vandersypen L, Wallraff A. NMR Quantum Computing. Stanford University; Stanford: USA. Available from: https://qudev.phys.ethz.ch/static/content/QSIT12/QSIT12_NMR_L01.pdf.
28. Bradley CE, Randall J, Abobeih MH, Berrevoets RC, Degen MJ, Bakker MA, et al. A ten-qubit solid-state spin register with quantum memory up to one minute. Phys Rev X. 2019; 9: 031045.
29. Jones JA. NMR-computation: A critical evaluation. Fortschr Phys. 2000; 48: 909-924.
30. He Y, Gorman SK, Keith D, Kranz L, Kaizer JG, Simmons NY. A two-qubit gate between phosphorous donor electrons in silicon. Nature. 2019; 571: 371-375.
31. Wallraff A, Schuster DI, Blais A, Frunzio L, Huang RS, Mejer J, et al. Strong coupling of a single photon to a superconducting qubit using circuit quantum electrodynamics. Nature. 2004; 431: 162-167.
32. Kjaergaard M, Schwartz ME, Braumüller J, Krantz P, Wang JIJ, Gustavsson S, et al. Superconducting qubits: Current state of play. Ann Rev Cond Matt Phys. 2020; 11: 369-395.
33. Katz N, Neely M, Ansmann M, Bilalczak RC, Hofheinz M, Lucero E, et al. Reversal of the weak measurement of a quantum state in a superconducting phase qubit. Phys Rev Lett. 2008; 101: 200401.
34. Kitaev AY. Fault-tolerant quantum computations by anyons. Ann Phys. 2003; 303: 2-30.
35. Riedinger R, Walucks A, Marinkovic I, Löschnauer C, Aspelmayer M, Hong S, et al. Remote quantum entanglement between two micromechanical oscillators. Nature. 2018; 556: 473-477.
36. Al-Khalili J, McFadden J. Life on the edge. The coming age of quantum biology. London: Bantam Press; 2014.
37. Ritz T, Thalau P, Phillips JB, Wiltscko R, Wiltschko W. Resonance effects indicate a radical-pair mechanism for avian magnetic compass. Nature. 2004; 429: 177-180.
38. Gauger EM, Rieper E, Morton JJL, Benjamin SC, Vedral V. Sustained quantum coherence and entanglement in the avian compass. Phys Rev Lett. 2011; 106: 040503.
39. Engel GS, Calhoun TR, Read EL, Ahn T-K, Macal T, Cheng YC, et al. Evidence for wavelike energy transfer through quantum coherence in photosynthetic systems. Nature. 2007; 446: 782-786.
40. Caruso F, Chin AW, Datta A, Huelga SF, Plenio MB. Highly efficient energy excitation transfer in light-harvesting complexes: The fundamental role of noise-assisted transport. J Chem Physics. 2009; 131: 105106.

Enjoy *Recent Progress in Materials* by:

1. Submitting a manuscript
2. Joining in volunteer reviewer bank
3. Joining Editorial Board
4. Guest editing a special issue

For more details, please visit:
http://www.lidsen.com/journals/rpm